RSC Advances

PAPER

View Article Online
View Journal | View Issue

Cite this: *RSC Adv.*, 2018, **8**, 42390

Characteristics of atomic layer deposited Gd_2O_3 on n-GaN with an AlN layer

Hogyoung Kim, *[a] Hee Ju Yun[b] and Byung Joon Choi*[b]

Received 26th November 2018
Accepted 14th December 2018

DOI: 10.1039/c8ra09708a

rsc.li/rsc-advances

The interfacial and electrical properties of atomic layer deposited Gd_2O_3 with an AlN layer on n-GaN were investigated. According to X-ray photoelectron spectroscopy spectra, the formation of Ga–O bonds that is significant near the Gd_2O_3/GaN interface was suppressed near the AlN/Gd_2O_3/GaN and Gd_2O_3/AlN/GaN interfaces. Larger amounts of oxygen atoms across the dielectric layers were observed for AlN/Gd_2O_3/GaN and Gd_2O_3/AlN/GaN junctions, which in turn produced the dominant peak corresponding to O–Al bonds. The flatband voltage shift in capacitance–voltage hysteresis characteristics was highest for the Gd_2O_3/AlN/GaN junction, indicating the highest interface and oxide trap densities. In addition, AlN/Gd_2O_3/GaN and Gd_2O_3/AlN/GaN junctions showed the highest interface state densities in the energy ranges of 0.1–0.2 eV and 0.4–0.6 eV, respectively. The reverse leakage currents were explained by Fowler–Nordheim (FN) for Gd_2O_3/GaN and AlN/Gd_2O_3/GaN junctions and by trap assisted tunneling (TAT) for the Gd_2O_3/AlN/GaN junction.

1. Introduction

Among rare earth (RE) oxide based materials, gadolinium oxide (Gd_2O_3) has been considered as a promising material for application in next-generation complementary metal–oxide–semiconductor (CMOS) transistors, because Gd_2O_3 has a wide band gap (~6.0 eV) with permittivity values of 10–14 for the epitaxial cubic phase, optimum band offset values with respect to Si, and high thermodynamic stability.[1–3] Gd_2O_3 has also been considered as a gate oxide in Ge-based MOS devices[4] and as a passivation layer for GaAs-based electronic devices.[5] Upon subjection to a forming gas treatment, the atomic layer deposition (ALD) grown Gd_2O_3 layer showed promising dielectric behavior, with no hysteresis and reduced interface trap density.[6]

Plasma-enhanced chemical vapor deposition (PECVD)-grown SiN_x has been used as an effective passivation material to suppress the current collapse in AlGaN/GaN metal–insulator–semiconductor heterostructure field-effect transistor (MIS-HFET).[7] High-k dielectric oxides such as Al_2O_3 and HfO_2 have also been employed as a passivation layer in AlGaN/GaN high electron mobility transistors (HEMTs).[8,9] However, it was shown that high density of deep (and slow) interface states exist near the Al_2O_3/(Al)GaN interface.[10,11] Hence, an alternative passivation method using an AlN layer has been considered for GaN-based devices.[12–14] It was demonstrated that the plasma enhanced atomic layer deposition (PEALD)-AlN as interfacial passivation layer is beneficial to improve the quality of Al_2O_3(HfO_2)/InGaAs interface, featuring good electrical characteristics and low interface trap density.[15,16] Wu *et al.* also observed similar passivation effect in Al_2O_3/GaN structure using a 2 nm thick AlN.[17] Due to the easy crystallization of AlN, however, the reverse leakage current become high when employing an AlN layer in the dielectric layer.

In our previous work, we found that the tunneling barrier height in Al_2O_3/GaN interface with a 1 nm thick AlN interlayer was lower than 1.0 eV, which could be due to the inferior Al_2O_3 film quality.[18] We also observed in Pt/AlN/n-GaN junctions with different AlN thicknesses that the formation of AlN layer near the AlN/GaN interface was observed clearly when the AlN thickness is above 1.5 nm.[19] These suggest that at least 2 nm thick AlN grown on GaN will be beneficial to passivate the GaN surface and to improve the overgrown film quality. Although molecular beam epitaxy (MBE) grown Gd_2O_3 on GaN has been investigated,[20,21] there is little knowledge regarding the interface characteristics of ALD-Gd_2O_3 on GaN. In this work, we comparatively investigated the interfacial and electrical properties of Gd_2O_3 on GaN with an AlN layer.

2. Experimental

Hydride vapor phase epitaxy (HVPE)-grown, n-type, c-plane (0001) GaN substrate (thickness: 300 μm, carrier concentration: 2×10^{17} cm^{-3}) purchased from Lumistal (Korea) was used in this work. After cutting the wafer into small pieces, some of them were loaded into a thermal ALD chamber (Atomic classic, CN-1, Korea) after cleaning process in a HCl : H_2O (1 : 1) solution, and three different methods to

[a]Department of Visual Optics, Seoul National University of Science and Technology (Seoultech), Seoul 01811, Republic of Korea. E-mail: hogyoungkim@gmail.com
[b]Departmet of Materials Science and Engineering, Seoul National University of Science and Technology (Seoultech), Seoul 01811, Republic of Korea. E-mail: bjchoi@seoultech.ac.kr

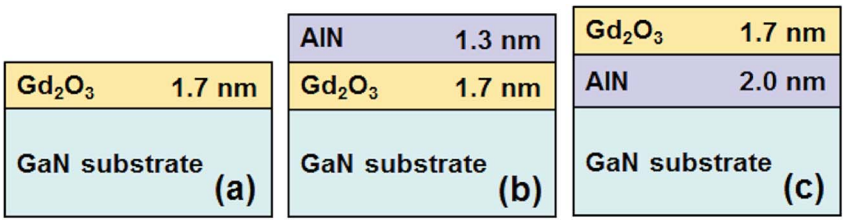

Fig. 1 Schematic layer structures of three samples denoted as (a) Gd_2O_3, (b) AlN/Gd_2O_3 and (c) Gd_2O_3/AlN.

deposit dielectric layers were applied on the prepared GaN substrates. (i) 1.7 nm thick Gd_2O_3 layer was directly deposited on the GaN surface at 250 °C with $(RCp)_2Gd(L)$ (Air Liquide, USA) as the Gd precursor and H_2O as the oxidant (denoted as Gd_2O_3). (ii) After depositing 1.7 nm thick Gd_2O_3 on the GaN surface using the same method in (i), the temperature was ramped up to 350 °C to deposit 1.3 nm thick AlN layer using trimethylaluminum (TMA) and NH_3 as precursors (denoted as AlN/Gd_2O_3). (iii) After depositing 2 nm thick AlN on the GaN surface using the same method in (ii), 1.7 nm thick Gd_2O_3 was deposited using the same method in (i) (denoted as Gd_2O_3/AlN). The schematic layer structures of three samples are presented in Fig. 1. The thicknesses of the films were measured using a FS-1 multi-wavelength ellipsometer (Film Sense, USA). Depth resolved X-ray photoelectron spectroscopy (XPS) measurements (PHI 5000 VersaProbe, ULVAC PHI, Japan) including sputter etch treatment were carried out using a monochromatic Al Kα X-ray source (beam energy: 1486.6 eV, spot size: 100 × 100 μm^2) to observe the chemical reaction near the dielectric/GaN interface. Due to charging effects that result in a shift in binding energy, the binding energy scale was calibrated by using the adventitious C 1s peak to 284.6 eV. The collected XPS data were analyzed using Multipak software. To characterize the electrical properties, metal–insulator–semiconductor (MIS) diodes were fabricated with a Pt Schottky electrode (diameter: 500 μm, thickness: 50 nm) and an Al back contact (thickness: 100 nm). Capacitance–voltage (*C–V*) and current–voltage (*I–V*) measurements were performed using a HP 4284A LCR meter and Keithley 238 current source, respectively. During the *C–V* measurements, an AC voltage of 30 mV with various frequencies was applied to the device so that small signal conditions were realized.

3. Results and discussion

After selecting the narrow scanned XPS spectra at one etch depth (thickness of the remained AlN: ~1.0 nm), we compared them each other to characterize the chemical reaction near the GaN surface. Fig. 2(a) shows the Ga $2p_{3/2}$ core-level spectra. The peaks at ~1117.1, ~1117.4, and ~1118.1 eV are associated with Ga_2O,[22] Ga_2O_3 [23] and GaN,[24] respectively. The integrated intensity ratios of Ga–O/Ga–N were calculated to be 1.98, 0.52, and 0.38, respectively, for the samples with Gd_2O_3, AlN/Gd_2O_3 and Gd_2O_3/AlN layers. This indicates that the suppression of Ga–O

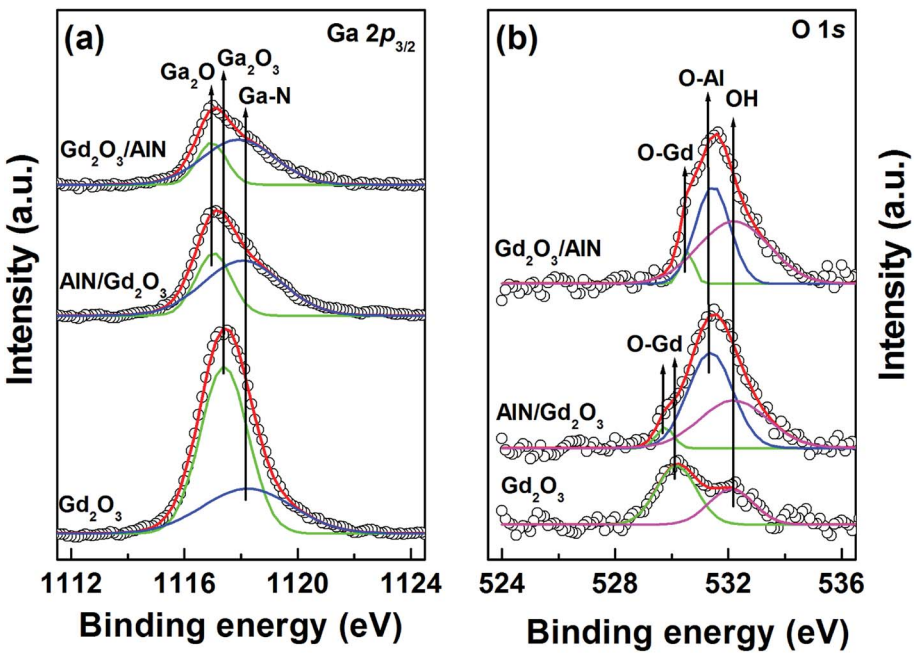

Fig. 2 XPS core level spectra of (a) Ga $2p_{3/2}$ and (b) O 1s for the samples with Gd_2O_3, AlN/Gd_2O_3 and Gd_2O_3/AlN layers after sputter etching. The thick of remained layer was about 1 nm.

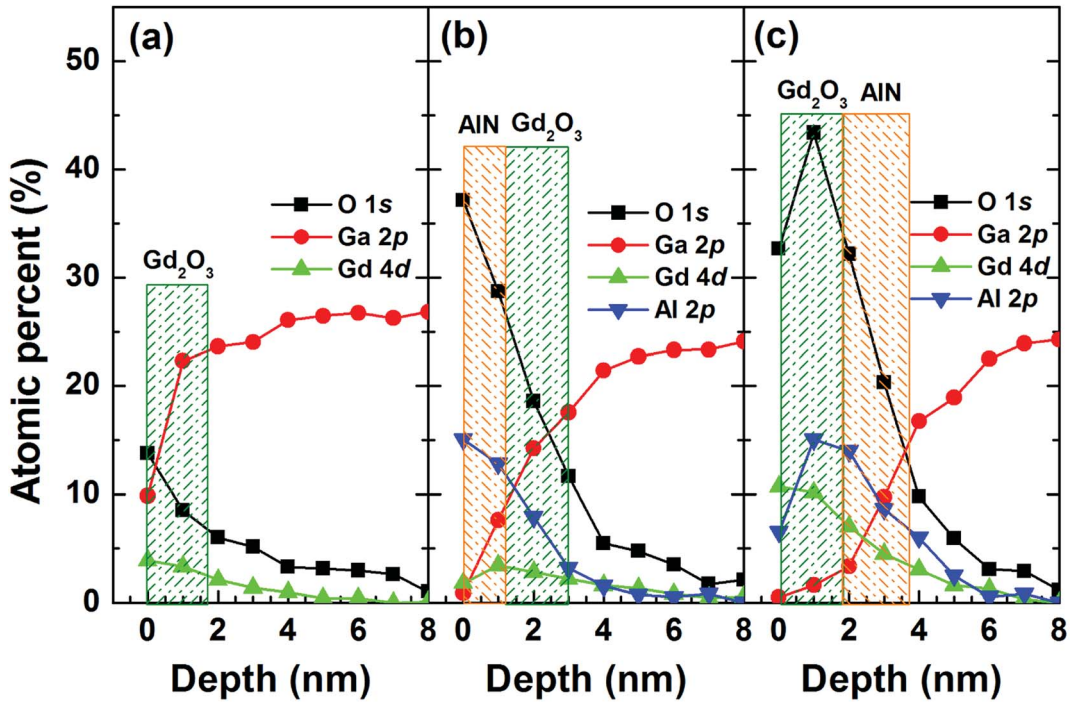

Fig. 3 XPS depth profiles for each element for the samples with (a) Gd_2O_3, (b) AlN/Gd_2O_3 and (c) Gd_2O_3/AlN layers.

bond occurred more significantly with a Gd_2O_3/AlN layer. Not Ga_2O_3 but Ga_2O was mainly observed for the samples with AlN/Gd_2O_3 and Gd_2O_3/AlN layers, indicating that Ga_2O_3 transferred into Ga_2O with thicker layers (so called, cleaning effect). It was shown in (In)GaAs based devices that a stable suboxide Ga_2O bond at the interface were not detrimental to device characteristics and the removal of Ga_2O_3 resulted in the reduction of frequency dispersion in capacitance.[25] As shown in Fig. 2(b), all three samples revealed a peak at ~532.5 eV, corresponding to O in the H_2O, OH^- impurities[26] and Gd hydroxides.[27] The emission peak at 529.8–530.2 eV could be associated with O in Gd_2O_3,[27] which became weak for the samples with AlN/Gd_2O_3 and Gd_2O_3/AlN layers. The integrated intensity ratios of [OH + O–Al]/O_{Total} were found to be 0.40, 0.95, and 0.95, respectively, for the samples with Gd_2O_3, AlN/Gd_2O_3 and Gd_2O_3/AlN layers. It was shown that Al–OH defects commonly observed in ALD-Al_2O_3 films is the origin of acceptor-like border traps and positive fixed charges in Al_2O_3.[28]

Fig. 3 shows the XPS depth profiles for each element obtained from the samples. The diffusion of Ga atoms into the overgrown layer was significant. The amount of oxygen atoms near the GaN surface is similar. However, both the samples with AlN/Gd_2O_3 and Gd_2O_3/AlN layers showed the larger amount of oxygen atoms across the overgrown layer as compared to the sample with Gd_2O_3 layer. This indicates that a significant portion of it resulted from the ALD deposition process itself. Fig. 4 shows the narrow scanned core level spectra from the sample surfaces (*i.e.*, without sputter etching). As shown in Fig. 4(a), the OH related peak observed for the samples with Gd_2O_3 and AlN/Gd_2O_3 layers is not observed for the sample with a Gd_2O_3/AlN bilayer. Along with the relatively weak peak at ~530.2 eV corresponding to O in Gd_2O_3, the additional peak at ~528.9 eV also appeared for the samples with Gd_2O_3 and Gd_2O_3/AlN layers, which could be associated with more oxidized Gd–O due to excess O and lattice defects.[29] Fig. 4(b) shows the Gd 4d core level spectra, which mainly originated from multiplet splitting of the 4d hole with 4f valence electrons to form 9D and 7D final ionic state.[30] As shown in Fig. 4(c), the peak related with AlN at 73.6–73.9 eV [31] is dominant for the sample with a Gd_2O_3/AlN bilayer whereas the peak associated with Al–O at ~74.6 eV [31] is dominant for the sample with an AlN/Gd_2O_3 bilayer. The additional peak at ~75.2 eV with a Gd_2O_3/AlN bilayer can be conformed to the Al–O chemical bond of Al_2O_3 or $Al(OH)_3$.[32]

Fig. 5(a)–(c) show the *C–V* curves measured at 1 kHz and 1 MHz. The frequency dispersion is hardly visible in the deep depletion region and small frequency dispersion is observed in the depletion, indicating the presence of interface states. The capacitance in accumulation at 1 kHz is much higher than that at 1 MHz, which can be due to current leakage through the dielectric layer which distorts the 1 kHz measurement.[33] The frequency dispersion in the accumulation region can also be associated with the formation of an inhomogeneous layer at the interface. Fig. 5(d)–(f) show the *C–V* hysteresis plots by sweeping the voltage from deep depletion to accumulation (up) and then accumulation to deep depletion (down). From the flatband capacitance (C_{FB}) obtained at each voltage sweep, the flatband voltage (V_{FB}) was calculated and then, the average interface and oxide trap density (Q_T) along the GaN bandgap (E_g) were obtained through $Q_T = (C_{OX}\Delta V_{FB})/qE_g$.[34] The trapped charge densities were calculated to be 3.68×10^9, 1.82×10^{11}, and 1.83×10^{12} cm^{-2} eV^{-1}, respectively, for the samples with Gd_2O_3, AlN/

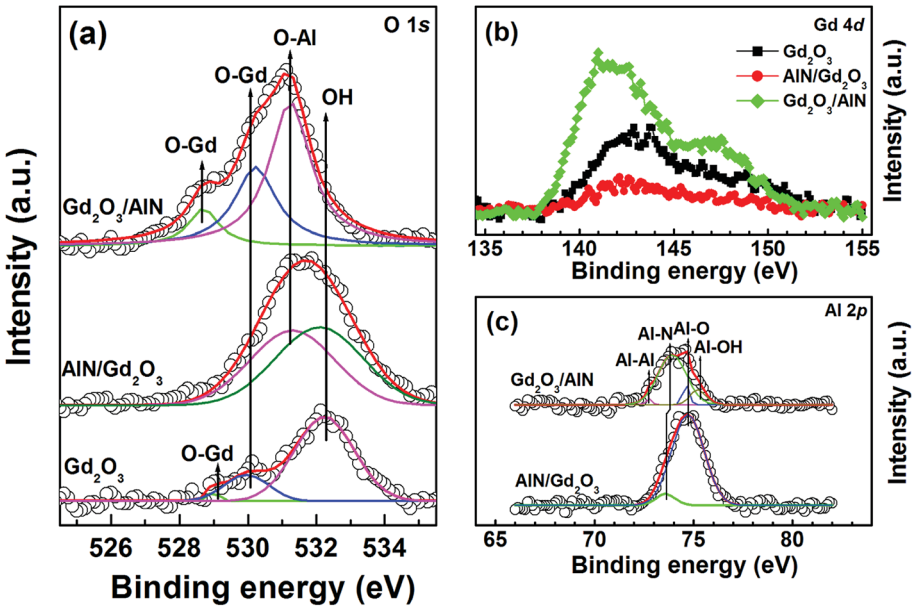

Fig. 4 XPS core level spectra of (a) O 1s, (b) Gd 4d and (c) Al 2p, which were obtained from the surface.

Gd_2O_3, and Gd_2O_3/AlN layers. The hysteresis can result from the interface states and oxide traps in the dielectric layer. Oxygen related defects are generated much with including an AlN layer (for example, see Fig. 2(b)). High density of Al–OH defects acting as acceptor-like border traps and positive fixed charges in Al_2O_3 may also increase the V_{FB} shift. Fig. 5(f) also shows that the C–V curves reveal a plateau region, reflecting the presence of 2 dimensional electron gas (2DEG) at the AlN/GaN interface.[35,36] With increasing the bias voltage, electrons start to accumulate at the channel interface, thus forming the 2DEG. An increase in capacitance is also observed at gate bias beyond +5 V. This is due to a charge spillover from the 2DEG channel, which brings some of the carriers closer to the surface, decreasing the effective barrier layer thickness and increasing the capacitance.[37]

Frequency dependent conductance–voltage measurements were performed to differentiate the types of the traps. The parallel conductance (G_p/ω) can be derived by $G_p/\omega = [\omega G_m(C_{OX})^2]/[(G_m)^2 + \omega^2(C_{OX} - C_m)^2]$, where C_m is the measured capacitance, G_m is the measured conductance, and C_{OX} is the oxide capacitance. The G_p/ω values as a function of radial frequency ($\omega = 2\pi f$) can be correlated with the trap density D_T and trap response time τ_T, given by[38]

$$\frac{G_p}{\omega} = \frac{qD_T}{2\omega\tau_T} \ln\left[1 + (\omega\tau_T)^2\right] \quad (1)$$

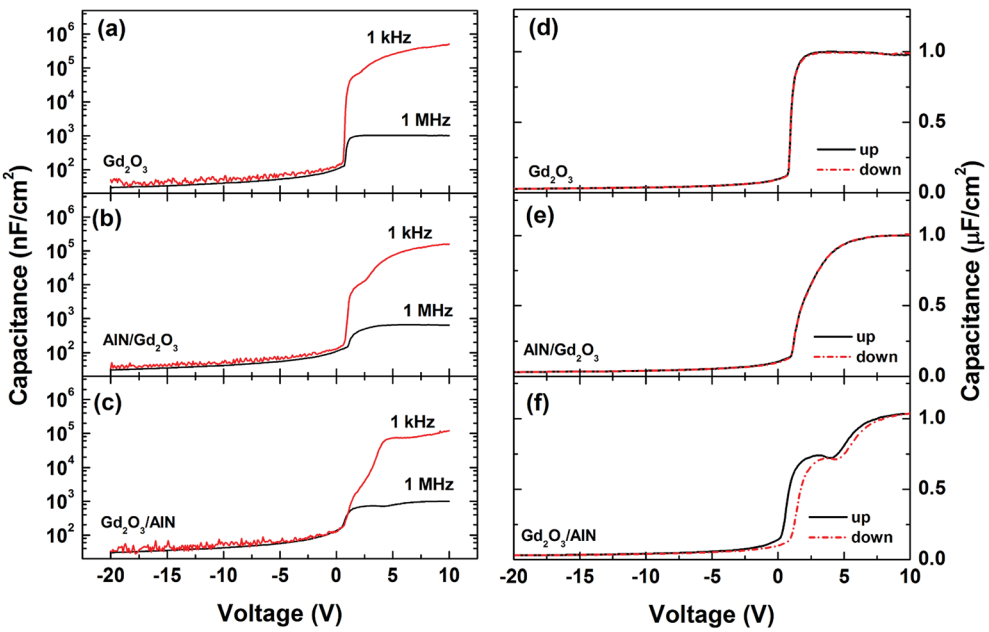

Fig. 5 (a)–(c) Capacitance–voltage (C–V) data measured at 1 kHz and 1 MHz and (d)–(f) C–V hysteresis plots measured at 1 MHz.

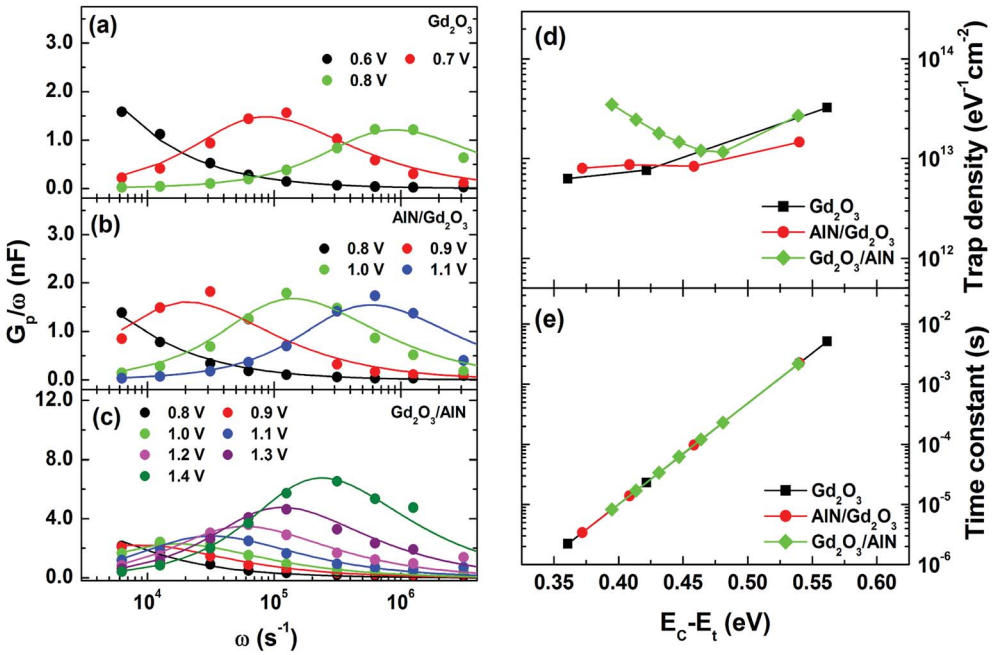

Fig. 6 Frequency dependent parallel conductance for the samples with (a) Gd_2O_3, (b) AlN/Gd_2O_3 and (c) Gd_2O_3/AlN, and (d) the obtained trap density and (e) the time constant from the conductance method.

The experimental and fitting data are shown in Fig. 6(a)–(c). The energy level of traps below the GaN conduction band, denoted as E_C–E_t (location of the trap energy) can be determined from τ_T according to the Shockley–Read–Hall statistics[39,40]

$$\tau_T = \frac{1}{v_{th}\sigma_n N_C} \exp\left(\frac{E_C - E_t}{kT}\right) \quad (2)$$

where v_{th} is the thermal velocity, σ_n is the electron capture cross section, and N_C is the effective density of states in the GaN conduction band. Using the values presented in ref. 40, the trap density and time constant as a function of energy level were calculated, which are shown in Fig. 6(d) and (e), respectively. According to the calculated time constants, the samples with Gd_2O_3 and AlN/Gd_2O_3 layers showed the wider distributions compared to the sample with a Gd_2O_3/AlN bilayer. Interestingly, the trap density at E_C–E_t = 0.38–0.47 eV showed the highest value for the sample with a Gd_2O_3/AlN bilayer. Hence, these traps can be considered to be from the AlN layer in the Gd_2O_3/AlN/GaN structure.

As shown in Fig. 7(a), an estimate of the interface state density (D_{it}) was made by applying Terman method to the experimental *C–V* curves measured at 1 MHz.[38] The obtained D_{it} *vs.* E_C–E_t plots in Fig. 7(b) revealed the lowest interface state density for the sample with a Gd_2O_3 layer. Interestingly, the samples with AlN/Gd_2O_3 and Gd_2O_3/AlN bilayers showed the highest interface state densities in the energy ranges of 0.1–0.2 eV and 0.4–0.6 eV, respectively. As shown in Fig. 3, large amount of Al atoms are present near the Gd_2O_3/GaN interface for the sample with an AlN/Gd_2O_3 bilayer. This might lead to the formation of AlN, leaving many nitrogen vacancies at the GaN surface. Fang *et al.* reported that several kinds of deep levels can be increased at the GaN surface after Cl_2-based inductively coupled plasma (ICP) etching.[41] In particular, they attributed a deep center located at E_C – 0.17 eV to nitrogen vacancy-related defect due to ICP etching. Yatabe *et al.* also showed in Al_2O_3/AlGaN/GaN structure that the *C–V* curves in the depletion region are stretched out more significantly to the positive direction when the interface state density peaked at E_C – 0.1 eV is higher.[42] Significant stretch out to the positive direction and high interface state density in the range of 0.1–0.2 eV observed for the sample with an AlN/Gd_2O_3 bilayer, thus, can be associated with the nitrogen vacancy-related defects. Meanwhile, Freedsman *et al.* showed in AlN/AlGaN/GaN MIS diodes that the trap density due to the AlN and AlGaN layers were located at 0.4–0.52 and 0.32–0.34 eV, respectively.[43] The energy distribution corresponding to the AlN insulating layer is similar to our work at the Gd_2O_3/AlN interface. Furthermore, Fig. 7(a) shows that flatband voltage shifted negatively for the sample with a Gd_2O_3 layer as compared to the sample with an AlN/Gd_2O_3 bilayer. It was shown that when Gd can only exist in the +3 oxidation state, the Gd_2O_3 cannot supply oxygen effectively to the dielectric/Si interface, which produced oxygen vacancies causing the negative shift in flatband voltage.[44] As shown in Fig. 2(b), the strong Gd_2O_3 related emission observed for the sample with a Gd_2O_3 layer was not observed for the sample with an AlN/Gd_2O_3 bilayer. Instead, the emission related with more oxidized Gd–O bond was observed. Therefore, it can be expected that oxygen vacancies have been reduced after depositing AlN layer with the excess O atoms.

Fig. 8(a) shows the typical semi-logarithmic current density–voltage (*J–V*) curves measured at room temperature. Compared to the sample with a Gd_2O_3 layer, the reverse leakage current increased for the samples with AlN/Gd_2O_3 and Gd_2O_3/AlN layers. Forward current at high bias region increased most

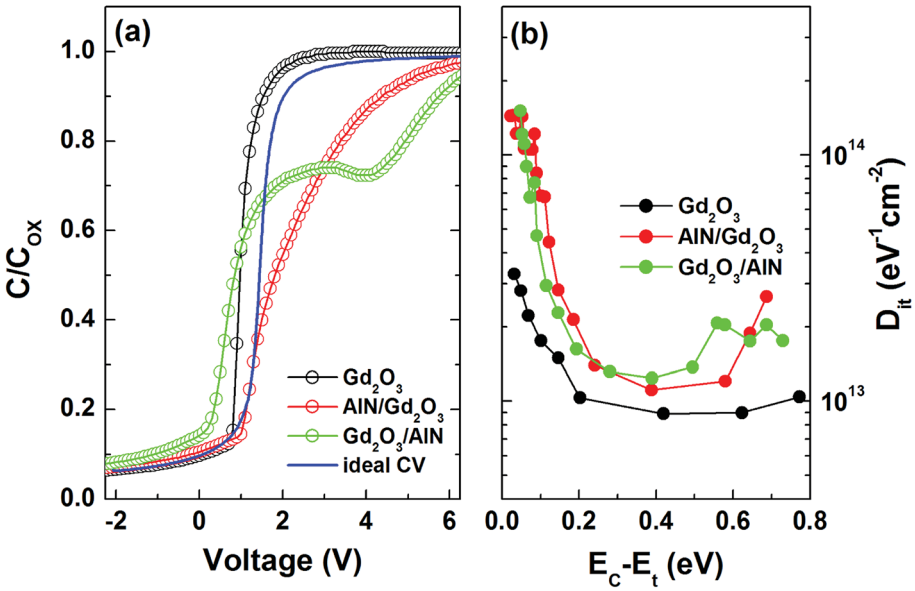

Fig. 7 (a) Comparison of experimental capacitance–voltage (C–V) data measured at 1 MHz and ideal C–V data and (b) interface state density (D_{it}) distributions determined by applying Terman method.

slowly for the sample with a Gd_2O_3/AlN bilayer, indicating the high series resistance. The reverse leakage current density at high bias region were analyzed using the Fowler–Nordheim (FN) tunneling model, given by[45]

$$J \propto E^2 \exp(-\beta/E) \quad (3)$$

where $\beta = 6.83 \times 10^{-7}(m^*)^{1/2}(\Phi_B)^{3/2}$, m^* is the effective electron mass in the insulator and Φ_B is the tunneling barrier height. As shown in Fig. 8(b), FN emissions were observed for the samples with Gd_2O_3 and AlN/Gd_2O_3 layers. The tunneling barrier heights (*i.e.*, conduction band offset at Gd_2O_3/GaN) were calculated to be about 1.95 and 1.36 eV, respectively, for the samples with Gd_2O_3 and AlN/Gd_2O_3 layers. Considering the reported value of 1.9 eV in Gd_2O_3/GaN interface,[46] the value for the sample with a Gd_2O_3 layer is very similar. Relatively lower value for the sample with an AlN/Gd_2O_3 bilayer may be due to the poorer interfacial quality as well as the interface and oxide traps.

Fig. 8(b) also shows that no FN emission was observed for the sample with a Gd_2O_3/AlN bilayer. Instead of FN emission,

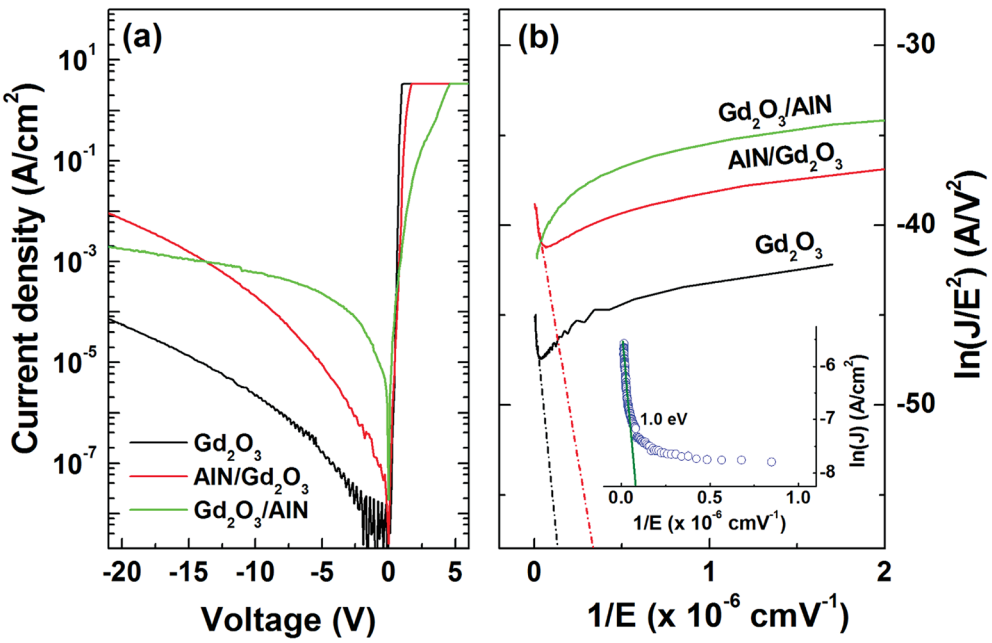

Fig. 8 (a) Typical semi-logarithmic current density–voltage (J–V) characteristics and (b) Fowler–Nordheim (FN) tunneling plots of ln(J/E^2) *vs.* 1/E. The inset in (b) presents trap assisted tunneling (TAT) plot of ln(J) *vs.* 1/E.

the trap assisted tunneling (TAT) was applied to the sample with a Gd_2O_3/AlN bilayer. In TAT emission, the reverse leakage current is given as $J \propto \exp(-\gamma/E)$, where $\gamma = 6.83 \times 10^{-7}(m^*)^{1/2}(\Phi_t)^{3/2}$ and Φ_t is the trap energy level, which can be obtained from the $\ln(J)$ *vs.* $1/E$ plot. From the linear fittings to the data as shown in the inset in Fig. 8(b), the trap energy level was estimated to be 1.00 eV. Energetically most favorable point defects in AlN are substitutional oxygen for nitrogen (O_N) and aluminum vacancy (V_{Al}), with the energy levels of ~0.8 and ~1.0 eV, respectively.[47] It was shown that dangling bonds in Al give rise to ~1.0 eV in energy level.[48] At present moment, it is suggested that Al related defects are responsible for TAT emission for the sample with a Gd_2O_3/AlN bilayer.

4. Conclusions

In conclusion, we investigated the interfacial and electrical properties of atomic layer deposited Gd_2O_3 with an AlN layer on n-GaN. X-ray photoelectron spectroscopy (XPS) spectra showed the dominant peaks associated with Ga–O and O–Al bonds, respectively, near the Gd_2O_3/GaN and AlN/Gd_2O_3/GaN and Gd_2O_3/AlN/GaN interfaces. Large amount of oxygen atoms across the dielectric layers were observed for the samples with Gd_2O_3/AlN and AlN/Gd_2O_3 layers. The highest flatband voltage shift in *C–V* hysteresis characteristics were observed for the sample with a Gd_2O_3/AlN bilayer, indicating the highest interface and oxide trap densities. According to parallel conductance and Terman methods, the samples with AlN/Gd_2O_3 and Gd_2O_3/AlN layers were found to have the highest interface state densities in the energy ranges of 0.1–0.2 eV and 0.4–0.6 eV, respectively. The reverse leakage currents for the samples with Gd_2O_3 and AlN/Gd_2O_3 layers were explained by Fowler–Nordheim (FN) whereas trap assisted tunneling (TAT) was more appropriate for the sample with a Gd_2O_3/AlN bilayer.

Conflicts of interest

There are no conflicts to declare.

Acknowledgements

This work was supported by Basic Science Research Program through the National Research Foundation of Korea (NRF) funded by the Ministry of Education (2017R1D1A1B03030400).

References

1 A. Laha, H. Osten and A. Fissel, *Appl. Phys. Lett.*, 2006, **89**, 143514.
2 H. Gottlob, T. Echtermeyer, M. Schmidt, T. Mollenhauer, J. Efavi, T. Wahlbrink, M. Lemme, M. Czernohorsky, E. Bugiel, A. Fissel, H. Osten and H. Kurz, *IEEE Electron Device Lett.*, 2006, **27**, 814.
3 K. Kukli, T. Hatanpää, M. Ritala and M. Leskelä, *Chem. Vap. Deposition*, 2007, **13**, 546.
4 V. Afanas'ev and A. Stesmans, *Mater. Sci. Semicond. Process.*, 2006, **9**, 764.
5 P. Yang, P. Ye, J. Kwo, M. Frei, J. Gossmann, J. Mannaerts, A. Sergent, M. Hong, K. Ng and J. Bude, *J. Cryst. Growth*, 2003, **251**, 837.
6 K. Xu, R. Ranjith, A. Laha, H. Parala, A. Milanov, R. Fischer, E. Bugiel, J. Feydt, S. Irsen, T. Toader, C. Bock, D. Rogalla, H. Osten, U. Kunze and A. Devi, *Chem. Mater.*, 2012, **24**, 651.
7 X. Hu, A. Koudymov, G. Simin, J. Yang, M. Asif Khan, A. Tarakji, M. Shur and R. Gaska, *Appl. Phys. Lett.*, 2001, **79**, 2832.
8 T. Hashizume, S. Ootomo and H. Hasegawa, *Appl. Phys. Lett.*, 2003, **83**, 2952.
9 J. Shi, L. Eastman, X. Xin and M. Pophristic, *Appl. Phys. Lett.*, 2009, **95**, 042103.
10 C. Mizue, Y. Hori, M. Miczek and T. Hashizume, *Jpn. J. Appl. Phys.*, 2011, **50**, 021001.
11 S. Huang, S. Yang, J. Roberts and K. Chen, *Jpn. J. Appl. Phys.*, 2011, **50**, 110202.
12 S. Huang, Q. Jiang, S. Yang, C. Zhou and K. Chen, *IEEE Electron Device Lett.*, 2012, **33**, 516.
13 S. Huang, Q. Jiang, S. Yang, Z. Tang and K. Chen, *IEEE Electron Device Lett.*, 2013, **34**, 193.
14 S. Zhao, X. Liu, L. Zhang, H. Huang, J. Shi and P. Wang, *Nanoscale Res. Lett.*, 2016, **11**, 137.
15 Q. Luc, E. Chang, H. Trinh, Y. Lin, H. Nguyen, Y. Wong, H. Do, S. Salahuddin and C. Hu, *IEEE Trans. Electron Devices*, 2014, **61**, 2774.
16 Q. Luc, H. Do, M. Ha, C. Hu, Y. Lin and E. Chang, *IEEE Electron Device Lett.*, 2015, **36**, 1277.
17 X. Wu, R. Liang, L. Guo, L. Lei, L. Xiao, S. Shen, J. Xu and J. Wang, *Appl. Phys. Lett.*, 2016, **109**, 232101.
18 H. Kim, D. Kim and B. Choi, *Appl. Phys. A*, 2017, **123**, 800.
19 H. Kim, H. Yoon and B. Choi, *Nanoscale Res. Lett.*, 2018, **13**, 232.
20 W. Chang, P. Chang, T. Lai, Y. Lee, J. Kwo, C. Hsu and M. Hong, *Cryst. Growth Des.*, 2010, **10**, 5117.
21 J. Johnson, B. Luo, F. Ren, B. Gila, W. Krishnamoorthy, C. Abernathy, S. Pearton, J. Chyi, T. Nee, C. Lee and C. Chuo, *Appl. Phys. Lett.*, 2000, **77**, 3230.
22 S. Wolter, B. Luther, D. Waltemyer, C. Önneby, S. Mohney and R. Molnar, *Appl. Phys. Lett.*, 1997, **70**, 2156.
23 F. Wang, K. Chen, C. Hsu, M. Liu and C. Yang, *Nanomaterials*, 2016, **6**, 88.
24 C. Hinkle, E. Vogel, P. Ye and R. Wallace, *Curr. Opin. Solid State Mater. Sci.*, 2011, **15**, 188.
25 C. Hinkle, M. Milojevic, B. Brennan, A. Sonnet, F. Aguirre-Tostado, G. Hughes, E. Vogel and R. Wallace, *Appl. Phys. Lett.*, 2009, **94**, 162101.
26 M. Li, D. Gao, S. Li, Z. Zhou, J. Zou, H. Tao, L. Wang, M. Xu and J. Peng, *RSC Adv.*, 2015, **5**, 104613.
27 S. Jeon and H. Hwang, *J. Appl. Phys.*, 2003, **93**, 6393.
28 J. Raja, C. Nguyen, C. Lee, N. Balaji, S. Chatterjee, K. Jang, H. Kim and J. Yi, *IEEE Electron Device Lett.*, 2016, **37**, 1272.
29 E. Külah1, L. Marot, R. Steiner, A. Romanyuk, T. Jung, A. Wäckerlin and E. Meyer, *Sci. Rep.*, 2017, **7**, 43369.

30 J. Gupta, D. Landheer, J. McCaffrey and G. Sproule, *Appl. Phys. Lett.*, 2001, **78**, 1718.
31 M. Alevli, C. Ozgit, I. Donmez and N. Biyikli, *Phys. Status Solidi A*, 2009, **2**, 266.
32 B. Brennan, R. Galatage, K. Thomas, E. Pelucchi, P. Hurley, J. Kim, C. Hinkle, E. Vogel and R. Wallace, *J. Appl. Phys.*, 2013, **114**, 104103.
33 R. Khosa, E. Thorsteinsson, M. Winters, N. Rorsman, R. Karhu, J. Hassan and E. Sveinbjörnsson, *AIP Adv.*, 2018, **8**, 025304.
34 C. Lee, H. Chen and H. Lee, *Appl. Phys. Lett.*, 2003, **82**, 4304.
35 M. Fagerlind, F. Allerstam, E. Sveinbjörnsson, N. Rorsman, A. Kakanakova-Georgieva, A. Lundskog, U. Forsberg and E. Janzén, *J. Appl. Phys.*, 2010, **108**, 014508.
36 T. Hashizume, S. Ootomo, T. Inagaki and H. Hasegawa, *J. Vac. Sci. Technol., B: Microelectron. Nanometer Struct.–Process., Meas., Phenom.*, 2003, **21**, 1828.
37 D. Cao, X. Cheng, Y. Xie, L. Zheng, Z. Wang, X. Yu, J. Wang, D. Shen and Y. Yu, *RSC Adv.*, 2015, **5**, 37881.
38 E. Nicollian and J. Brews, *MOS Physics and Technology*, John Wiley & Sons, New York, 1982.
39 D. Schroder, *Semiconductor Material and Device Characterization*, Wiley, New York, 2005.
40 S. Liu, S. Yang, Z. Tang, Q. Jiang, C. Liu, M. Wang, B. Shen and K. Chen, *Appl. Phys. Lett.*, 2015, **106**, 051605.
41 Z. Fang, D. Look, X. Wang, J. Han, F. Khan and I. Adesida, *Appl. Phys. Lett.*, 2003, **82**, 1562.
42 Z. Yatabe, J. Asubar, T. Sato and T. Hashizume, *Phys. Status Solidi A*, 2015, **212**, 1075.
43 J. Freedsman, T. Kubo and T. Egawa, *Appl. Phys. Lett.*, 2011, **99**, 033504.
44 S. Dueñas, H. Castán, H. García, A. Gómez, L. Bailón, K. Kukli, T. Hatanpää, J. Lu, M. Ritala and M. Leskelä, *J. Electrochem. Soc.*, 2007, **154**, G207.
45 H. Lin, P. Ye and G. Wilk, *Appl. Phys. Lett.*, 2005, **87**, 182904.
46 J. Robertson and B. Falabretti, *J. Appl. Phys.*, 2006, **100**, 014111.
47 C. Stampfl and C. van de Walle, *Phys. Rev. B*, 2002, **65**, 1.
48 C. Wu and A. Kahn, *Appl. Phys. Lett.*, 1999, **74**, 546.